Liquid Crystals
Publication details, including instructions for authors and subscription information:
http://www.informaworld.com/smpp/title~content=t713926090

Viscosities of a bent-core nematic liquid crystal

E. Dorjgotov[a]; K. Fodor-Csorba[b]; J. T. Gleeson[c]; S. Sprunt[c]; A. Jákli[a]
[a] Chemical Physics Interdisciplinary Program, Liquid Crystal Institute, Kent State University, Kent, OH 44242 [b] Research Institute for Solid State Physics and Optics, Hungarian Academy of Sciences, Budapest, Hungary [c] Department of Physics, Kent State University, Ohio, 44242

To cite this Article Dorjgotov, E. , Fodor-Csorba, K. , Gleeson, J. T. , Sprunt, S. and Jákli, A.(2008) 'Viscosities of a bent-core nematic liquid crystal', Liquid Crystals, 35: 2, 149 — 155
To link to this Article: DOI: 10.1080/02678290701824199
URL: http://dx.doi.org/10.1080/02678290701824199

Liquid Crystals,
Vol. 35, No. 2, February 2008, 149–155

Taylor & Francis
Taylor & Francis Group

Viscosities of a bent-core nematic liquid crystal

E. Dorjgotov[a], K. Fodor-Csorba[c], J. T. Gleeson[b], S. Sprunt[b] and A. Jákli[a]*

[a]*Chemical Physics Interdisciplinary Program, Liquid Crystal Institute, Kent State University, Kent, OH 44242, USA;* [b]*Department of Physics, Kent State University, Kent, Ohio, 44242, USA;* [c]*Research Institute for Solid State Physics and Optics, Hungarian Academy of Sciences, Budapest, Hungary*

(Received 28 September 2007; final form 23 November 2007)

Viscosity measurements are reported for a bent-core nematic liquid crystal, 4- chloro-1,3-phenylenebis{4-[4′-(9-decenyloxy)benzoyloxy]} benzoate (ClPbis10BB). The rotational viscosity was measured by analysing the dynamics of director rotation in pulsed magnetic fields, and the flow viscosities were determined by employing a new electro-rotation technique. The results show that whereas the rotational viscosity is more than ten times larger than for calamitic liquid crystals, the flow viscosity is more than 100 times larger. Even more striking is the difference between the ratio of the flow and rotational viscosities, which for calamitic nematics is typically 0.1, whereas in this bent-core material it is ~50. This suggests that the large shear viscosity is primarily due not so much to the molecular size, but rather the shape. A model is discussed that may explain the observations.

Keywords: viscosity; bent-core nematic

1. Introduction

Liquid phases exhibiting purely orientational order (nematic phases) are rather uncommon in bent-core compounds, because the kinked geometry of the molecules strongly frustrates disorder. Nonetheless, a number of new bent-core compounds exhibiting nematic phases (BCNs) have recently been synthesised (*1*). Simultaneously there has been a surge in theoretical studies (*2*) predicting intriguing new thermotropic nematic and isotropic structures including biaxial phases, orientationally ordered but optically isotropic phases and even spontaneously chiral and polar liquid phases. Experimental studies of the BCN materials have indicated spontaneous and induced biaxiality (*3*) and giant flexoelectric effects (*4*), which promise not only novel physics but also opportunities for new technical applications. Dynamic light scattering (*5*), electrohydrodynamic instabilities (*6*), magnetic field-induced birefringence (*7*) and NMR measurements (*8*) on BCNs indicate that their properties are unconventional both in the nematic and isotropic phases. The most comprehensive studies have been carried out on the bent-core nematic liquid crystal substance 4-chloro-1,3-phenylenebis-{4-[4′-(9-decenyloxy)benzoyloxy]}benzoate (ClPbis10BB) (*9*). Although its dielectric and Frank elastic constants ($\Delta\varepsilon \sim -1.6$, $K_{11} \sim K_{33} \sim 2.3 \times 10^{-12}$ N) and the diamagnetic anisotropy ($\chi_a = 1.7 \times 10^{-7}$ (SI) are typical for calamitic liquid crystals (*6*), the leading Landau coefficient is 30 times lower, the viscosity associated with nematic order fluctuations is ten times higher (*10*), the conductivity anisotropy is two orders of magnitude lower (*6*) and the flexoelectric coefficient is three orders of magnitude larger (*4*) than typically observed in calamitic rod-shaped liquid crystals. We have also noted that filling sandwich-type cells with these materials via capillary action takes more than an hour instead of less than one minute for typical liquid crystals, indicating either anomalously high flow viscosity or unusually low wetting properties. To clarify this we report studies of both the flow and rotational viscosities of ClPbis10BB. For the rotational viscosity measurements the pulsed magnetic field method (*11*) was used. For the measurement of the flow viscosities we chose a novel 'electro-rotation' technique recently described for smectic liquid crystals (*12*). Unlike traditional shear flow experiments (*13, 14*), this technique requires only a small amount of material, does not rely on uniform alignment over large areas and allows one to locally probe rheological properties. These advantages are especially important for the study of BCN materials, which are not yet commercially available. Because the electro-rotation technique has not been tested in calamitic nematic materials, for control purposes we first tested the technique on a commercially available calamitic nematic liquid

*Corresponding author. Email: jakli@lci.kent.edu

ISSN 0267-8292 print/ISSN 1366-5855 online

DOI: 10.1080/02678290701824199
http://www.informaworld.com

crystal mixture (ZLI 3640 from Merck), which exhibits a stable nematic phase with negative dielectric anisotropy at room temperature.

2. Experiments

For the electro-rotation measurements a small number of glass cylinders (small enough that the average distance between cylinders is many times larger than their length) of diameter ranging from 4.5 μm to 7.0 μm were dispersed in liquid crystal cells with cell thicknesses of around 12 μm. Experiments on ClPbis10BB were carried out under both dc and ac fields at various temperatures in both the nematic and isotropic phases; ClPbis10BB is crystalline at room temperature and has a stable nematic phase between 60°C and 73°C and is optically isotropic above 73°C. The control calamitic mixture was tested at room temperature under dc fields.

The cell substrates were treated with uni-directionally rubbed polyimide (PI2555 from Dupont), which was observed to induce uniform planar alignment for both rod-shape and bent-core liquid crystals. Both liquid crystals have negative dielectric anisotropy, which prevents them from switching under the applied electric field. Dielectric constants and conductivities of the liquid crystals were obtained by measuring the frequency and temperature dependence of complex impedance with a precision LCR meter (Quadtech, model 1920). Rotational motion of the fibre spacers was recorded by a DVD recorder and was analysed on a computer.

The measurements of director dynamics in pulsed magnetic fields of ClPbis10bb were carried out in homogeneously aligned 55 μm thick samples, which were placed between the pole faces of an electromagnet. The director distortion was tracked by measuring the capacitance of the liquid crystal layer using an Andeen-Hagerling AH2500 autobalancing bridge; the capacitance was monitored as a function of time after an abrupt jump (either up or down) of the magnetic field. The magnet power supply was capable of changing the field within about six seconds; this was sufficiently quick, as the relaxation time (as is shown below) was much longer.

3. Results

Electro-rotation measurements

At zero electric field, uniform textures appeared (see Figure 1a), even near the cylinders in both materials. For ZLI 3640 this remained true even when electric fields were applied, whereas in case of the bent-core material, an inhomogeneity appeared above a frequency dependent threshold (Figure 1b). Slightly above the threshold, stripes appeared along the rubbing direction, which coincide the long axes of the majority of cylinders. At even higher fields the texture becomes chaotic (see Figure 1c), and finally optically isotropic (*9*).

Snapshots of the electric field-induced rotation of glass cylinders in the calamitic liquid crystal ZLI3640 are shown in Figure 2. The different stages of cylinder rotation can be judged by the orientation of the end face, which is not perpendicular to the long axis. High-frequency rotation indicates low viscosity, which is typical for calamitic nematic liquid crystals.

Figure 3 shows the measured angular frequency of the cylinder versus applied field for ZLI3640.

In case of the BCN, under dc fields, rotation began only at high fields and once it started an electrohydrodynamic instability was set up, obscuring a clear view of the cylinder. For this reason we employed ac fields with which electro-rotation could be clearly observed in the 10 Hz to 100 Hz frequency regime. Snapshots of rotation of a glass cylinder in ClPbis10bb liquid crystal are shown in Figure 4. One can see from the time indicators that the rotational frequency is dramatically lower for the bent-core than for the calamitic nematic material, in spite of the much higher temperature. This shows that the bent-core liquid crystal has much higher viscosity than of a regular nematic or it is visco-elastic.

The frequency dependency of the electro-rotation at constant electric field of $E_0 = 2.7\,\mathrm{V\,\mu m^{-1}}$ was measured at different temperatures. The results are plotted in Figure 5. After rising abruptly at low frequencies, the angular velocity reaches a maximum around 20–25 Hz, then slowly decreases to zero at 60 Hz (70°C) or at 100 Hz (72°C).

The rotational frequency as the function of the squared electric field amplitude at frequency 20 Hz is shown in Figure 6. It can be seen that the characteristic response is not linear over all amplitudes; a relatively sharp increase of the slopes can be observed above a temperature dependent threshold indicating a drop in the viscosity. This threshold coincides with the threshold for the formation of chaotic texture, which becomes optically isotropic at higher fields. Note that the nonlinearity disappears when the material is in isotropic phase at $T = 77$°C (see inset to Figure 6).

Pulsed field measurements

We monitored the capacitance of the liquid crystal as a function of time after abruptly either increasing or decreasing the magnetic field (starting at $t = 0$) from

Figure 1. Textures of 12 µm thick ClPbis10BB film around 6.4 µm diameter glass rods between crossed polarizers with λ = 106 nm wave-plate inserted: (a) E=0 V µm^{-1}, (b) E=3.3 V µm^{-1} and (c) 10.5 V µm^{-1} f=80 Hz sinusoidal electric field waveforms applied.

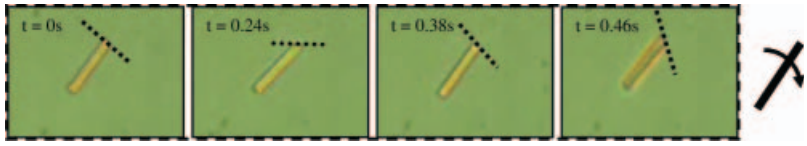

Figure 2. Snapshots of glass cylinder dispersed in calamitic nematic liquid crystal, ZLI 3640, at different time steps with dc field amplitude: E≈1.0 V µm^{-1} (12 µm cell with 6 µm spacers). Pictures were taken between uncrossed polarizers. The rotation around the long axis of the molecules can be seen by following the rotation of the direction of one of the edge (indicated by dotted line to guide the eye) that is slanted with respect to the long axis.

well below (or above) to well above (or below) the threshold field for the splay Freedericksz transition, as shown in Figure 7. When the field is increased and the director goes from being uniform to splay-distorted, the capacitance evolves following a stretched exponential time dependence with time constant of 43 s and stretching parameter of about 0.4. This behaviour is different from the expected simple exponential change (*11*).

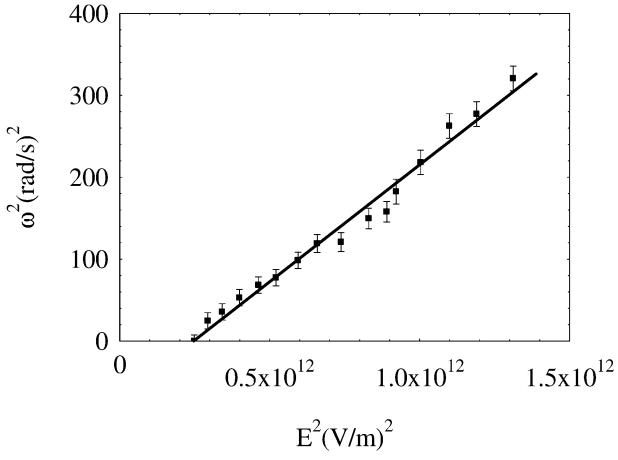

Figure 3. Square of the angular velocity of 4.5 µm diameter glass cylinder dispersed in nematic liquid crystal ZLI 3640 as a function of the square of applied dc field.

Even more unexpected is the observation that when the magnetic field is removed, the relaxation to the uniform state proceeds by a two-stage process. As can be seen in the 'relaxation process' data in Figure 7, both processes can be fitted by single exponential with time constants of τ_1=357 s and τ_2=204 s.

4. Discussion

A dc electric field-induced steady rotation of solid spherical objects in isotropic liquids was first observed in 1893 by Weiler (*15*) [and termed 'Quincke rotation' (*16*)], but was explained only in 1984 by Jones (*17*). In the first description of Quincke rotation in liquid crystals it was demonstrated that by proper analysis of the rotation one can determine one or more Miesowicz viscosity coefficients (*18*) in smectic liquid crystals (*12*). First we show that the same analysis applies also in the nematic phase.

The electro-rotation of particles under dc fields is usually described by the effective dipole moment approach analysed for spherical particles (*17*). Adopting this theory for slender cylinders (*19*), the time-averaged electric torque can be calculated as:

$$\langle T^e \rangle = 4V\varepsilon_1 E_0^2 \frac{\varpi\sigma_1\sigma_2(\tau_2-\tau_1)}{(\sigma_1+\sigma_2)^2(\varpi^2\tau_{mw}^2+1)}, \qquad (1)$$

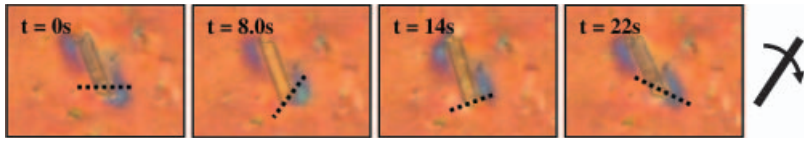

Figure 4. Snapshots of 4.5 μm diameter glass cylinder dispersed in bent core nematic liquid crystal, at different time steps. Square wave, $E \approx 10.0\,\mathrm{V\,\mu m^{-1}}$ at $f=20$ Hz. $T=70^{\circ}$C. The 12 μm thick cell is viewed with inserted wave-plate. The rotation around the long axis of the molecules can be seen by following the rotation of the direction of one of the edge (indicated by dotted line to guide the eye) that is slanted with respect to the long axis.

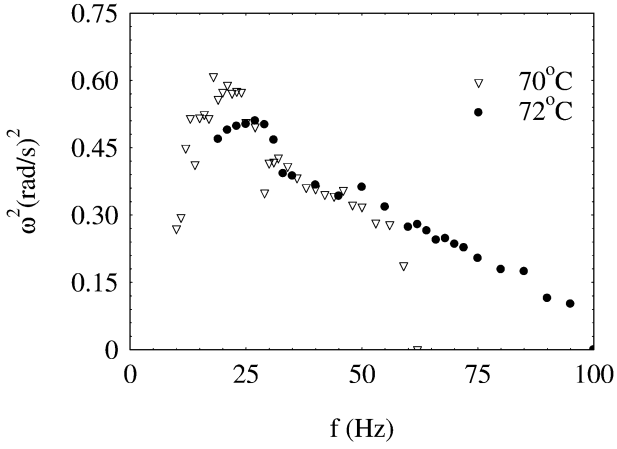

Figure 5. Angular velocity of the 4.5 μm diameter glass cylinder dispersed in the bent-core nematic liquid crystal as function of the frequency of applied field, $E_0=2.7\,\mathrm{V\,\mu m^{-1}}$.

where E_0 is the externally applied field, σ_1 (ε_1) and σ_2 (ε_2) are the electric conductivity (static dielectric constant) of the fluid and glass particles, respectively, and $\tau_{mw}=\frac{\varepsilon_1+\varepsilon_2}{\sigma_1+\sigma_2}$ is the Maxwell–Wagner charge relaxation time. The flow viscosity η corresponding to the Miesovicz coefficients η_c for homeotropic and η_a or η_b (whichever is smaller) for planar alignment, can be calculated from measuring the angular velocity, ω, of the steady rotation from the condition that $\langle T^e\rangle=-\langle T^\eta\rangle=4V\eta\omega$.

It is important to mention that electro-rotation appears only if the relaxation time of the particle, τ_2, is greater than that of the liquid, τ_1. This means the conductivity of the particle must be smaller than that of the fluid. As was shown by Liao *et al.* (*12*) in the limit where conductivity of the particle is much less than that of the fluid, the angular frequency simplifies to

$$\omega=\frac{E_c^2\varepsilon_2}{\eta(1+\varepsilon_2/\varepsilon_1)}\sqrt{\frac{E_0^2}{E_c^2}-1}, \qquad (2)$$

where E_c is the critical field where the rotation starts. Although this formula requires measuring both E_c and ω, the significance of it is that it does not contain the conductivity values which are very sensitive to impurities and would provide different values for each sample.

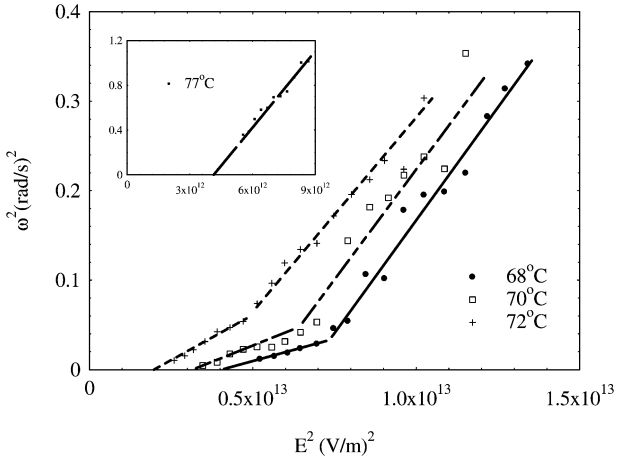

Figure 6. Angular velocity of the glass cylinder dispersed in bent-core liquid crystal as function of applied field squared (square wave with $f=20$ Hz). Main panel: behaviour in nematic phase indicating two different viscosities depending on the measuring field; insert: in the isotropic phase there is no break in the slope indicating field-independent viscosity.

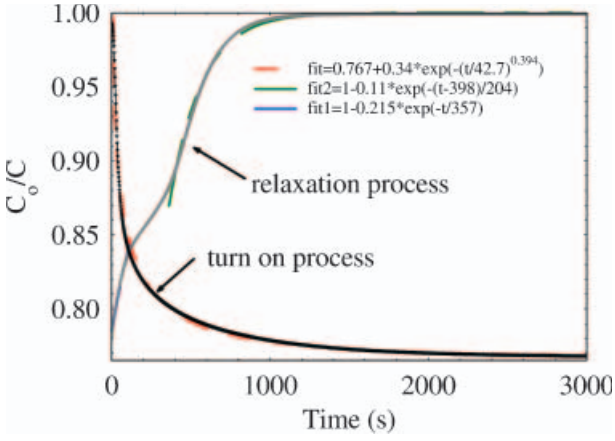

Figure 7. Capacitance (relative to undistorted state) of homogeneously aligned ClPbis10BB vs. time after an abrupt change of magnetic field (at $t=0$). C decreases with increasing field because $\Delta\varepsilon$ is negative. When a field is applied, the capacitance (and hence the director) changes following a stretched exponential time variation. When the field is removed, the director relaxation unfolds following an unprecedented two-stage process.

Due to the dielectric nature of the material the torque is a quadratic function of the electric field ($\langle T^e \rangle \propto \sim E^2 = E_0^2 \cos^2 \omega_0 t$), which means that applied sinusoidal fields result in both dc and double frequency torques with amplitudes half of the base frequency amplitude, because $\cos^2 \omega_o t = \frac{1}{2}(1 + 2\cos(2\omega_o t))$. The angular frequency of the induced rotation due to the ac field therefore has the same form as Equation (2), but with the scaling corresponding to $E_0^2 \rightarrow \frac{1}{2} E_0^2$ and $E_c^2 \rightarrow \frac{1}{2} E_c^2$. Here we note that these arguments are different from Turcu's bifurcation theory (*20*), which predicts no rotation in our system, as discussed in the appendix. Also, it is found that electro-rotation under ac fields is possible only at angular frequencies where the ions can follow the electric field, i.e. at values smaller than the inverse of the Maxwell–Wagner relaxation time.

Besides these notions we need to keep in mind that the effect of free ions will become important when one uses insulating layers to align the liquid crystal. In this case the free ions will partially screen out the external electric field up to a field E_{sc}, which can be related to the electric conductivity of the liquid crystal as (*21*)

$$E_{sc} = \frac{q n_0 d}{\varepsilon_0 \varepsilon_1} \approx \frac{\sigma_1 k_B T d}{q D \varepsilon_0 \varepsilon_1}. \tag{3}$$

After the rescaling of E_0 and E_c and the introduction of the screening field E_{sc}, our final equation used for the analysis of the electric field dependence of angular frequency of the ac field-induced cylinder rotation becomes

$$\omega = \frac{E_c^2 \varepsilon_2}{2\eta(1 + \varepsilon_2/\varepsilon_1)} \sqrt{\frac{E_0^2 - 2\frac{\sigma_1 k_B T d}{q D \varepsilon_0 \varepsilon_1}}{E_c^2} - 1}. \tag{4}$$

The measured maximum of the induced rotation at around 20 Hz applied ac field (see Figure 5) is due to two competing effects: at low frequencies the free ions in the fluid migrate to screen out the applied field below $f_c \approx \frac{1}{2\pi d} \sqrt{\frac{\sigma_1 D}{\varepsilon_0 \varepsilon_1}}$ (*21*), whereas at high frequencies above the Maxwell–Wagner frequency ($f^{MW} = 1/\tau_{MW}$) the dipole cannot build up at the colloid surfaces. Remarkably, the measured physical parameters ($\sigma_1 \sim 10^{-8}\,(\Omega\,\mathrm{m})^{-1}$, $\varepsilon_1 \sim 8$, $\varepsilon_2 = 3.9$) provide $f_{MW} \sim 100$ Hz and $f_c \sim 10$ Hz, thus explaining that the electro-rotation drops below $f_c \sim 10$ Hz and above 100 Hz.

Although in previous electro-rotation studies on smectics (*12*) E_{sc} was much smaller than E_c and hence could be neglected, in the case of nematic liquid crystals (such as ZLI 3640 with $\sigma \sim 10^{-9}\,(\Omega\,\mathrm{m})^{-1}$, $d = 12\,\mu\mathrm{m}$, $D \sim 10^{-11}\,\mathrm{m^2\,s^{-1}}$, $\varepsilon_1 \sim 10$ and $T \sim 300$ K), E_{sc} is about $0.3\,\mathrm{V\,\mu m^{-1}}$, which is in the same order of magnitude as that of the critical field $E_c \sim 0.5\,\mathrm{V\,\mu m^{-1}}$. To obtain the correct viscosity, therefore, one needs to replace E_c with E_c–E_{sc}. Taking this into account, the flow viscosity of ZLI 3640 becomes 0.05 Pa s, which agrees with the manufacturer's value (*22*). Due to the higher temperature range of the bent-core nematic ClPBis10BB, the measured conductivity and dielectric constants give a larger screening field of $E_{sc} \sim 1\,\mathrm{V\,\mu m^{-1}}$.

Armed with this analysis, we can determine the flow viscosity of the bent-core material ClPBis10BB from the rescaled Equation (2). The results are shown in Figure 8, where we see several interesting features. First of all, the flow viscosity of the bent-core material is over 100 times larger than of the conventional calamitic nematic materials, which explains why it takes over an hour to fill the cell by capillary action in the isotropic phase. Secondly, the viscosity measured at high fields corresponds to that measured in the lower temperature isotropic phase indicating that this is the $\alpha_4/2$ component of the Leslie coefficients (*21*) due to the isotropic director distribution that appears in the field induced chaotic texture.

The viscosity measured in low fields corresponds to a uniform texture where the director is perpendicular to the shear plane which shows this viscosity component corresponds to the Miesowicz viscosity η_a (*21*). The jump in the flow viscosity observed at about 4°C above the first clearing point indicates an evolution in isotropic structure. A similar, though somewhat weaker jump in the viscosity associated with nematic order fluctuations has been observed in dynamic light scattering studies (*22*). The jumps in the two viscosities can be explained by local development of optically isotropic clusters of molecules, a

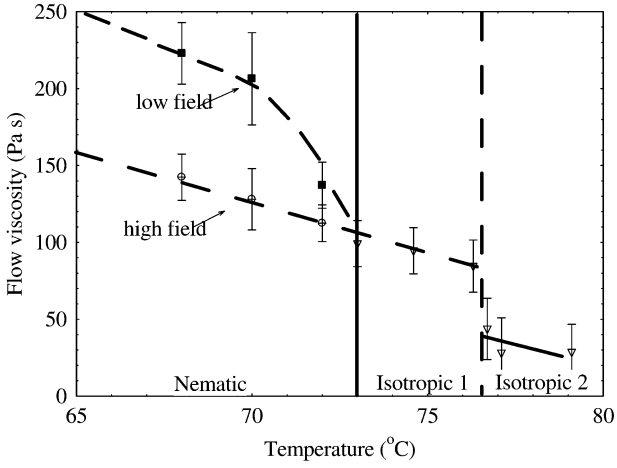

Figure 8. Calculated shear viscosity of bent-core liquid crystal ClPBis10BB as a function of temperature.

model recently suggested on the basis of a wide range of experimental results obtained on the isotropic phase of ClPbis10BB (*23*).

The rotational viscosity of the material can be determined from the decay time τ_d obtained from the fit to the time dependence of the capacitance upon turning off the magnetic field by the expression (*11*) $\gamma_1 = \frac{\tau_d \pi^2 K_{11}}{d^2}$. From the previously measured (*6*) $K_{11} = 2.23 \times 10^{-12}$ N we obtain $\gamma_1 \sim 2.6$ Pa s for the first part of the relaxation process, and $\gamma_1 \sim 1.5$ Pa s for the second. Both of these rotational viscosity values are more than an order of magnitude larger than in rod-shaped molecules like pentylcyanobiphenyl or methoxybenzylidenebutylaniline, the same order of increase that was reported in light scattering studies of director fluctuations in ClPbis10BB (*5*).

An even more striking difference between calamitic and bent-core nematics is the ratio of rotational and flow viscosities $\Gamma = \gamma_1/\eta$. In calamitic nematics (*22*) $\Gamma_c \sim 10$, whereas in this bent-core material $\Gamma \sim 0.02$. This shows that the large shear viscosity is not primarily due to the increased size of the bent-core molecule relative to typical calamitics, but rather due to the shape differences of the molecules. Whereas rod-shape molecules can translate during shear flow, bent-shape molecules experience a steric barrier by passing each other. This may promote the formation of temporary clusters, which explains the gooey consistency of the material even in the isotropic phase. Such a clustering has been suggested by several studies (*7, 8*) though the exact size, shape and temporal behaviour of the clusters are not known.

Both the flow and rotational viscosity measurements strongly support the clustering hypothesis and lead us to suggest a preliminary model that can account for both the stretched exponential variation of the capacitance when the magnetic field is turned on and the double relaxation process when the field is removed. For this we utilise the fact that the ground state is characterised by a negative dielectric anisotropy $\varepsilon_a(0)$ and positive diamagnetic anisotropy $\chi_a(0)$. When the magnetic field is applied across the film the clusters turn toward the magnetic field and simultaneously deform so that they become more elongated with $\chi_a(H) > \chi_a(0)$ and $|\varepsilon_a(H)| > |\varepsilon_a(0)|$. When the field is removed, the rotation of the director starts only after some delay, because there is a degeneracy in which direction the director can rotate, and first only the shape of the aggregates relax back to the a less elongated form with $\chi_a(0)$ and $\varepsilon_a(0)$. This results in the plateau at an intermediate capacitance range. The capacitance then eventually reaches the original value only as the director rotates back to the configuration dictated by the planar alignment layer. This model has to be verified by additional measurements, and at this stage we cannot exclude the possibility that this behaviour could be caused by an unexpectedly large difference between viscosity coefficients. Furthermore, more accurate techniques, such as used by Svensek and Zumer (*24*) for rigorously solving the Ericksen–Leslie equations, may also yield the observed behaviour.

In summary, we have presented experimental results of an unprecedented ratio of flow to orientational viscosity, which not only validate extending the electro-rotation technique to nematic liquid crystals, but also reveal unexpected and intriguing phenomena when applied to bent-core nematics. In addition, pulsed-field measurements of orientational dynamics cannot be described by the usual single-exponential relaxation. We have also proposed a physical model based on cluster formation, deformation and rotation, which is consistent with the observations.

Acknowledgements

The work was supported by NSF Grant DMR-0606160 and by the Hungarian Science Research Fund, OTKA K-61075. Technical assistance was provided by X. Zhou.

References

(1) (a) Matraszek J.; Mieczkowski J.; Szydlowska J.; Gorecka E. *Liq. Cryst.* **2000**, *27*, 429–436; (b) Wirth, I.; Diele, S.; Eremin, A.; Pelzl, G.; Grande, S.; Kovalenko, L.; Pancenko, N.; Weissflog, W. *J. Mater. Chem.* **2001**, *11*, 1642–1650; (c) Weissflog, W.; Nádasi, H.; Dunemann, U.; Pelzl, G.; Diele, S.; Eremin, A.; Kresse, H. *J. Mater. Chem.* **2001**, *11*, 2748–2758; (d) Mátyus, E.; Keserű, K. *J. Mol. Struct.* **2001**, *543*, 89–98; (e) Dingemans, T.J.; Samulski, E.T. *Liq. Cryst.* **2000**, *27*, 131–136.

(2) (a) Lubensky T.C.; Radzihovsky L. *Phys. Rev. E* **2002**, *66*, 031704-1–27; Radzihovsky L.; Lubensky T.C. *Europhys. Lett.* **2001**, *54*, 206–212; (b) Brand, H.R.; Pleiner, H.; Cladis, P.E. Eur. Phys. J. E **2002**, *7*, 163–166; (c) Dozov, I. *Europhys. Lett.* **2002**, *56*, 247.

(3) (a) Acharya B.R.; Primak A.; Kumar S. *Phys. Rev. Lett.* **2004**, *92*, 145506; Madsen, L.A.; Dingemans, T.J.; Nakata, M.; Samulski, E.T. *Phys. Rev. Lett*. **2004,** *92,* 145505; (b) Olivares, J.; Stojadinovic, S.; Dingemans, T.; Sprunt, S.; Jákli, A. *Phys. Rev. E* **2003**, *68*, 041704-1–6.

(4) Harden J.; Mbanga B.; Éber N.; Fodor-Csorba K.; Sprunt S.; Gleeson J.T.; Jákli A. *Phys. Rev. Lett.* **2006** *97*, 157802.

(5) Stojadinovic S.; Adorjan A.; Sprunt S.; Sawade H.; Jakli A. *Phys. Rev. E* **2002**, *66*, 060701.

(6) Wiant D.B.; Gleeson J.T.; Eber N.; Fodor-Csorba K.; Jákli A.; Toth-Katona T. *Phys. Rev. E* **2005**, *72*, 041712.

(7) Wiant D.; Stojadinovic S.; Neupane K.; Sharma S.; Fodor-Csorba K.; Jákli A.; Gleeson J.T.; Sprunt S. *Phys. Rev. E* **2006**, *73*, 030703(R).

(8) Domenici V.; Veracini C.A.; Zalar B. *Soft Matter* **2005**, *1*, 408; Cinacchi, G.; Domenici, V. *Phys. Rev. E* **2006**, *74*, 030701.
(9) Fodor-Csorba K.; Vajda A.; Galli G.; Jákli A.; Demus D.; Holly S.; Gács-Baitz E. *Macromol. Chem. Phys* **2002**, *203*, 1556.
(10) Wiant D.; Stojadinovic S.; Neupane K.; Sharma S.; Fodor-Csorba K.; Jákli A.; Gleeson J.T.; Sprunt S. *Phys. Rev. E* **2006**, *73*, 030703.
(11) Pieranski P.; Brochard F.; Guyon E. *J. Phys., Paris* **1972**, *34*, 35; de Gennes, P.G.; Prost, J. *The Physics of Liquid Crystals*; Oxford University Press: Oxford, 1993.
(12) Liao G.; Smalyukh I.I.; Kelly J.R.; Lavrentovich O.D.; Jákli A. *Phys. Rev. E* **2005**, *72*, 031704.
(13) Horn R.G.; Kleman M. *Ann. Phys. (Paris)* **1978**, *3*, 229; Battacharya, S.; Letcher, S.V. *Phys. Rev. Lett.* **1980**, *44*, 414.
(14) Larson R.G. *The Structure and Rheology of Complex Fluids*; Oxford University Press: Oxford, 1999.
(15) Weiler W. *Z. Phys. Chem. Unterricht* **1893**, Heft IV, 194 (A).
(16) Quincke G. *Ann. Phys. Chem.* **1896**, *11*, 27.
(17) Jones T.B. *IEEE Trans. IAS* **1984**, *1A-20*, 845; Jones, T.B. In *Electromechanics of Particles*; Cambridge University Press: New York, 1995.
(18) Miesowicz M. *Nature* **1935**, *17*, 261.
(19) Feng J.Q. *J. Colloid Interface Sci* **2002**, *246*, 112.
(20) Turcu I. *J. Phys. A* **1987**, *20*, 3301–3307.
(21) Jákli A.; Saupe A. *One- and Two-dimensional Fluids*; Taylor and Francis: New York, 2006.
(22) Merck, *Liquid Crystal Mixtures for Electro-optic Displays;* EM Industries, Inc: 1994.
(23) Wiant D.; Neupane K.; Sharma S.; Jákli A.; Gleeson J.T.; Sprunt S.; Pradhan N.; Iannachione G. *submitted to Phys. Rev. Lett.* **2007**.
(24) Svensek D.; Zumer S. *Continuum Mech. Thermodyn* **2002**, *14*, 231.

Appendix

Turcu's bifurcation model operates by decomposing the applied field into right and left circularly polarised fields, E_+ and E_-. Adapting this model to cylindrical particles we calculated the dc component of the electric torque as

$$\langle T^e \rangle = V\varepsilon_1 E_0^2 \frac{\varepsilon_r - \sigma_r}{(1+\sigma_r)(1+\varepsilon_r)} \left(\frac{\chi+\chi_0}{(\chi+\chi_0)^2+1} + \frac{\chi-\chi_0}{(\chi-\chi_0)^2+1} \right), \quad (5)$$

where

$$\varepsilon_r = \frac{\varepsilon_2}{\varepsilon_1}, \sigma_r = \frac{\sigma_2}{\sigma_1}, \chi = \varpi\tau_{mw}, \chi_0 = \varpi_0\tau_{mw}. \quad (6)$$

From this the steady state solution of rotating cylinder subject to ac field can be given as

$$\omega_\pm^2 = \frac{1}{2\tau_{MW}^2} \left(\frac{E_0^2}{E_c^2} + 2\left(\chi_0^2 - 1\right) \pm \sqrt{\left(\frac{E_0}{E_c}\right)^4 - 16\chi_0^2} \right). \quad (7)$$

We see that these solutions do not contain information about the viscosity, which only enters in the time needed to reach the steady state. In fact stability analysis shows (*17, 20*) that when $\omega_0\tau_{\mathrm{MW}} \gg 1$ and $\tau_2 > \tau_1$ (which is the case for liquid crystal–glass cylinder systems), the steady rotation frequency is zero. We conclude, therefore, that Turcu's bifurcation model (*20, 17*) does not provide any rotation in our system under ac field excitation.